Summer 5-26-2017

Joint Monitoring of Pipeline-Flood Based on FBG and Zigbee Technologies

Bing Han
China National Institute of Standardization, China, hanb@cnis.gov.cn

Qiang Fu
China National Institute of Standardization, China

Hanfang Hou
China National Institute of Standardization, China

Jingjuan Zhang
China National Institute of Standardization, China

Joint Monitoring of Pipeline-Flood Based on FBG and Zigbee Technologies

Bing Han[*], *Qiang Fu*, *Hanfang Hou*, *Jingjuan Zhang*
China National Institute of Standardization, China

Abstract: A joint monitoring system of pipeline-flood on the basis of FBG and ZigBee is designed in this article by applying fiber Bragg grating sensing into hydrologic observation and mechanical vibration measurement field, which can realize multipoint and online monitoring of rainfall, river level, flow velocity and vibration frequency of pipeline. The influence of temperature on measurement results can be eliminated by using the dual-fiber pattern. In order to achieve the real-time and effective performances of data collection, the monitoring system is built on the basis of ZigBee wireless network system, which consists of the sensor nodes equipped with the FBG ombrometer, FBG fluviograph, FBG flowmeter and FBG vibrometer in the monitoring area, and they are connected to a network coordinator in a star topology structure. The communication between the ZigBee system and remote monitoring terminal has been realized by GPRS modules. This monitoring system has been put into practical application on a gas pipeline laid in a river valley. The experiment results have proved that the system has the characteristics of flexible and fast networking, real-time capability, low power consumption, high reliability and unattended operation, which can meet the requirements of safety monitoring of oil and gas pipelines subjected to flood impacting.

Keywords: flood, oil and gas pipeline, FBG, ZigBee, joint monitoring

1. INTRODUCTION

Long-distance oil and gas pipelines laid in river valley are always suffered flood scouring, riverbed degradation, stream bank erosion, debris flow and etc. These hydrotechnical geohazards may cause the buried pipelines to be exposed out of earth surface and result in suspended span, which brought serious threatens to pipeline operation [1]. In order to obtain the hydrological regime and safety condition of pipelines, we have designed a joint monitoring device of pipeline-flood based on fiber Bragg grating, which is a type of optical fiber passive device and formed by creating periodical distribution of refraction index in fiber core based on the photosensitive characteristics of fiber material, and it has the advantages of anti-electromagnetic interference, waterproof, wide dynamic range, high sensitivity, convenient to build up network and easy to realize distributed measurement [2]. It is reported that there are lots of quantities can be measured by using FBG sensing technology, such as temperature [3]-[4], strain [5], concentration [6], current [7], magnetic field [8], pressure [9], acceleration [10], stress [11], vibration [12], voltage [13], and so on. In order to ensure data validation, consistency and real-time property, the wireless sensor network is built to centralize the monitoring information of multipoint to the field monitoring stations based on ZigBee technology, and it can be realized that the real-time monitoring of hydrological regime and pipelines by communication with the remote monitoring terminal through network center node of ZigBee with GPRS.

2. PRINCIPLE OF FBG SENSING

The changes in temperature or strain can cause the changes in period and refractive index of FBG, and then lead to the changes in reflection spectrum and transmission spectrum of FBG. We can obtain the variation values of temperature and strain by detecting reflection spectrum and transmission spectrum of FBG. When the ambient temperature, strain, or other physical quantities change, the grating period Λ or fiber core refractive index n_{eff} will change, and the reflection spectrum and transmission spectrum of FBG will change as well, which will

* Corresponding author. Email:hanb@cnis.gov.cn(Bing Han)

cause the center wavelength of the fiber grating to occur a displacement $\Delta\lambda$, as shown in Figure 1.

Based on the coupled mode theory, a guided mode which is propagated in uniform FBG may be coupled to another one propagated in the opposite direction to form a narrow-band reflection, and the peak reflection wavelength λ_B can be written as follow [14]

$$\lambda_B = 2n_{eff}\Lambda \tag{1}$$

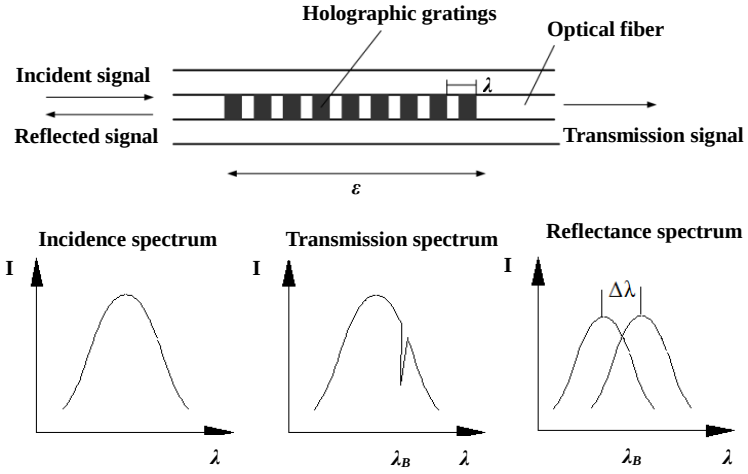

Figure. 1 Schematic diagram of FBG sensing principle

Where, λ_B is Bragg wavelength, n_{eff} is effective refractive index of fiber transmission mode, Λ is grating pitch. We can get wavelength shift of FBG, λ_B, which is caused by strain ε and temperature difference ΔT by differential transformation with respect to Eqs. (1), as follow [15]

$$\frac{\Delta\lambda_B}{\lambda_B} = \left(\alpha_f + \xi\right)\Delta T + \left(1 - P_e\right)\varepsilon \tag{2}$$

Where, α_f, ζ and P_e are the thermal expansion coefficient, thermo-optical coefficient and elasto-optical coefficient of fiber optic materials. It can be seen from Eqs. (2) that the change of Bragg wavelength is influenced by strain ε due to the elastic-optic effect of FBG and the temperature T due to the thermal expansion effect. In order to eliminate the impact of temperature change on the measurement results of fiber grating, the double FBGs design is adopted, that the two fiber grating sensors are adhered to the measured object with longitudinal symmetrical structure, and both the two Bragg wavelength shifts of fiber grating caused by temperature change are the same, while both of them caused by strain change are equal in magnitude but opposite in direction, so Eqs. (2) can be expressed as follow

$$\frac{\Delta\lambda_{B1}}{\lambda_B} = (\alpha_f + \xi)\Delta T + (1 - P_e)\varepsilon \tag{3}$$

$$\frac{\Delta\lambda_{B2}}{\lambda_B} = (\alpha_f + \xi)\Delta T - (1 - P_e)\varepsilon \tag{4}$$

Combining Eqs. (3) and Eqs. (4), we have

$$\frac{\Delta\lambda_B}{\lambda_B} = \frac{\Delta\lambda_{B1} - \Delta\lambda_{B2}}{\lambda_B} = 2(1 - P_e)\varepsilon \tag{5}$$

3. STRUCTURE AND PRINCIPLE OF MONITORING DEVICE

This monitoring device is made up of four monitoring units: FBG ombrometer, FBG fluviograph, FBG flowmeter and FBG vibrometer, which are respectively responsible for the data acquisition of rainfall, river level, flow velocity and vibration frequency of pipeline.

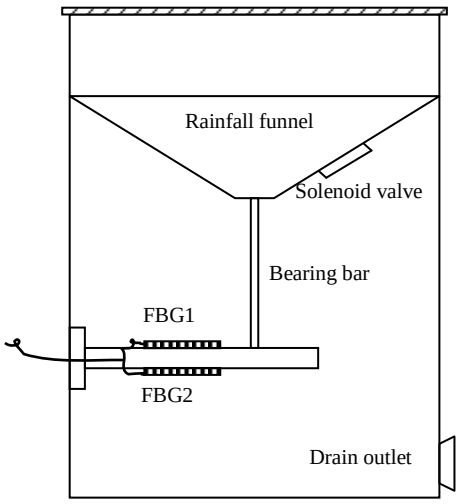

Figure 2. Structure diagram of FBG ombrometer

3.1 FBG ombrometer

The FBG ombrometer is constituted of the rain cylinder, rain funnel, bearing bar, cantilever beam, FBG strain sensors, solenoid valve and drain outlet, and the double fiber Bragg grating, FBG1 and FBG2, are adhered to cantilever beam with longitudinal symmetrical structure, as is shown in Figure 2.

When it start to rain in monitoring regional, with the gradual accumulation of rainwater in cylinder, the rain funnel will slide downward along the cylinder wall under the gravity of rainwater, and the gravity of rainwater will be transmitted to cantilever beam through bearing bar, which causes the cantilever beam bending. According to material mechanics, the axial strain of cantilever beam, ε, can be written as follows

$$\varepsilon = \frac{6\rho v g L}{Ebt^2} \tag{6}$$

The rainfall q can be expressed by precipitation depth per unit area, as follows

$$q = \frac{v}{A} = \frac{4v}{\pi d^2} \tag{7}$$

Combining Eqs. (5), Eqs. (6) and Eqs. (7), we have

$$\frac{\Delta\lambda_B}{\lambda_B} = \frac{3\pi\rho g L d^2}{Ebt^2}(1-P_e)q \tag{8}$$

Where, ρ is the density of water, g is the gravity acceleration, d is the diameter of cylinder, L, t, b and E are the length, thickness, width and elasticity modulus of beam. Based on Eqs. (8), the rainfall q can be measured indirectly by using the FBG ombrometer.

In order to achieve the function of automatic drainage, the FBG ombrometer is equipped with a solenoid valve which is controlled by the micro controller unit (MCU). When the volume of rainwater in cylinder has reached the receiving limit of the FBG ombrometer, the MCU will send a pulse signal to the solenoid to control the valve is opened, and the valve will be closed automatically after the rainwater is drained off.

3.2 FBG fluviograph

The constitution of FBG fluviograph is shown in Figure 3, its main body is an airtight waterproof box with a thin-wall steel tube inside it, and two FBG strain sensors are adhered to the monitoring cross-section of steel tube symmetrically.

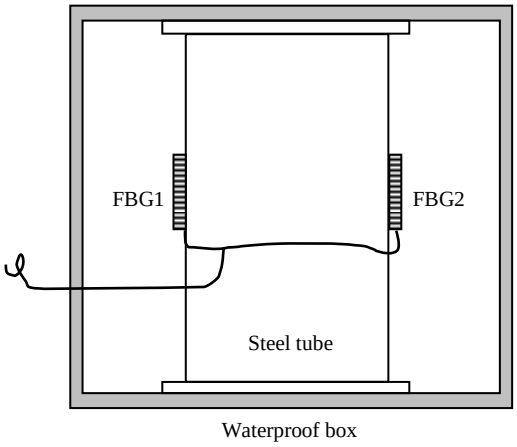

Figure 3. Diagrammatic drawing of FBG fluviograph

According to hydrostatics, the hydro-static pressure P at a depth of h, can be written as follow

$$P = P_0 + \gamma h \tag{9}$$

Where P_0 is the atmospheric pressure, γ is the unit weight of water. The hydro-static pressure P will change in the case of water level change. The deformation will occur on waterproof box due to the change of hydro-static pressure P, which leads to the thin-wall steel tube fixed in box producing axial strain. Based on theory of elastic mechanics, Eqs. (9) can be written as follow

$$P = E\varepsilon \tag{10}$$

Where E is the elastic modulus of thin-wall steel tube, ε is the strain on monitoring cross-section of steel tube.

Combining Eqs. (5), Eqs. (9) and Eqs. (10), we have

$$\frac{\Delta\lambda_B}{\lambda_B} = 2(1-P_e)\frac{P_0 + \gamma h}{E} \tag{11}$$

Based on Eqs. (11), the river level h can be measured indirectly by using the FBG fluviograph.

3.3 FBG flowmeter

The FBG flowmeter mainly includes two parts, the venturi tube and pressure sensing device based on fiber grating, they are connected to each other with two conduits, as is shown in Figure 4. On the basis of principle of fluid mechanics, when flux density is constant, the Bernoulli equation of incompressible fluid can be written as follow

$$P_1 + \frac{1}{2}\rho v_1^2 = P_2 + \frac{1}{2}\rho v_2^2 \tag{12}$$

Based on fluid continuity equation, we have

$$\pi\left(\frac{1}{2}d_1\right)^2 v_1 = \pi\left(\frac{1}{2}d_2\right)^2 v_2 \tag{13}$$

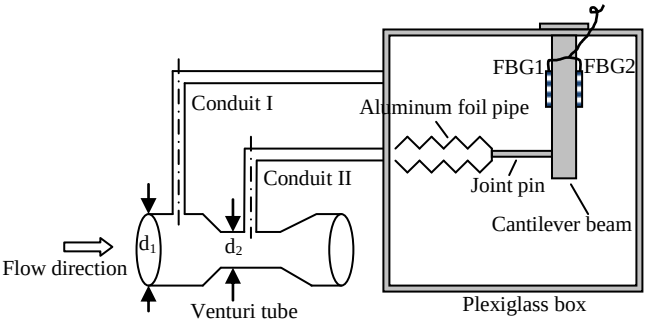

Figure 4. Schematic diagram of FBG flowmeter

By combining Eqs. (12) and Eqs. (13), the pressure difference between the cross-section of conduit I and conduit II can be deduced, as follow

$$\Delta P = P_1 - P_2 = \frac{\rho}{2}\left[\left(\frac{d_1}{d_2}\right)^4 - 1\right]v^2 \tag{14}$$

Where, d_1 and d_2 are the inner diameters of venture tube; v_1, v_2, and P_1, P_2, are the flow velocity and pressure on longitudinal section of conduit I and conduit II; ρ is fluid density; $v=v_1$.

As is known from Eqs. (14), the flow velocity of fluid has a positive correlation with pressure difference between conduit I and conduit II, and the pressure difference ΔP can be measured with the pressure sensing device based on fiber grating whose main body is a plexiglass box with an aluminum foil pipe and a cantilever beam inside it, and they are connected by a joint pin; two FBG sensors are adhered to cantilever beam with longitudinal symmetrical structure.

Based on material mechanics theory, the axial strain of cantilever beam ε meets the following formulas

$$\varepsilon = \frac{6hFl}{Ebh^3} \tag{15}$$

Where E, h, l and b are the elasticity modulus, thickness, length and width of beam, F is the pressure force applied to beam. Because the aluminum foil pipe is stretchable only along axial direction and its elasticity coefficient is very small, F can be expressed as follow

$$F = \Delta PSg = \frac{\pi d^2 g}{4}\Delta P \tag{16}$$

Where ΔP is the pressure difference inside and outside of aluminum pipe, S is the cross-section area of pipe, g is acceleration of gravity, d is the pipe diameter.

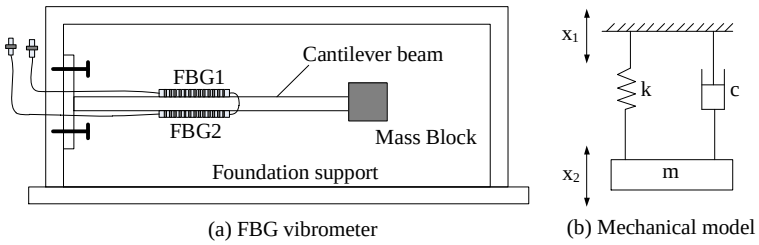

(a) FBG vibrometer (b) Mechanical model

Figure 5. Schematic diagram of FBG vibrometer

Combining Eqs. (5), Eqs. (14), Eqs. (15) and Eqs. (16), we have

$$\frac{\Delta\lambda_B}{\lambda_B} = \frac{3(1-P_e)\pi\rho g l d^2}{2Ebh^2}\left[\left(\frac{d_1}{d_2}\right)^4 - 1\right]v^2 \tag{17}$$

Based on Eqs. (17), the flow velocity v can be measured indirectly by using the FBG flowmeter.

3.4 FBG vibrometer

The design of FBG vibrometer can be achieved by sticking two FBG sensors on cantilever beam with symmetrical structure, as shown in Figure 5a); the vibration mechanical model can be simplified as a forced vibration structure system with second order single degree of freedom as shown in Figure 5b), wherein m is a mass block of the system, k is the elastic coefficient of FBG, c is the damping coefficient of system.

When the system is under external force, assuming that the absolute displacement of foundation support is x_1, and the absolute displacement of mass block is x_2, based on Newton's second law of motion, the differential equations of FBG vibrometer can be written as follow

$$mx_2^{''} + c(x_2^{'} - x_1^{'}) + k(x_2 - x_1) = 0 \tag{18}$$

What the fiber grating has detected is x, the relative change between mass block and foundation support, if we let $x = x_2 - x_1$, then Eqs. (18) can be written as follow

$$mx^{''} + cx^{'} + kx = -mx_1^{''} \tag{19}$$

Assuming that the motion form of foundation support is a simple harmonic vibration with amplitude A and angular frequency ω under external force, the vibration displacement can be expressed as follow

$$x_1 = a\sin\omega t \tag{20}$$

Combining Eqs. (19) and Eqs. (20), we have

$$x^{''} + 2\xi\omega_n x^{'} + \omega_n^2 x = a\omega^2 \sin\omega t \tag{21}$$

Where, ξ is the damping ratio, ω_n is the natural vibration frequency, and the steady-state solution of Eqs. (21) can be defined as follow

$$x = A\sin(\omega t - \varphi) \tag{22}$$

Where A is amplitude-frequency characteristic, φ is phase-frequency characteristic. Assuming that the outside excitation frequency is far less than natural vibration frequency, then Eqs. (21) can be simplified as follow

$$x \approx \frac{1}{\omega_n^2} x_1^{''} \tag{23}$$

Where ω_n can be written as follow

$$\omega_n = \sqrt{\frac{k}{m}} = \sqrt{\frac{Ebt^3}{6ml^3}} \tag{24}$$

For the cantilever beam in Figure 5a), based on the theory of material mechanics, we have

$$\varepsilon = \frac{xt}{l^2} \tag{25}$$

Combining Eqs. (5), Eqs. (23), Eqs. (24) and Eqs. (25), we have

$$\frac{\Delta\lambda_B}{\lambda_B} = 2(1 - P_e)\frac{6ml}{Ebt^2} x_1^{''} \tag{26}$$

Based on Eqs. (26), the vibration acceleration can be measured indirectly by using the FBG vibrometer. After the vibration acceleration is processed by using the *Fast Fourier Transform* computation method, the amplitude and frequency at measuring point can be obtained based on the wave number in the quarter period.

4. DESIGN OF MONITORING SYSTEM

4.1 System composition

As is shown in Figure 6, the monitoring system is composed of the following three components:

• ZigBee wireless sensor network. It consists of the sensor nodes equipped with the FBG ombrometer, FBG fluviograph, FBG flowmeter and FBG vibrometer in the monitoring area, and they are connected to a network coordinator in a star topology structure. The monitoring data acquired by each sensor node is sent wirelessly to the network coordinator, and the coordinator is connected to a GPRS module via RS-232 port [16].

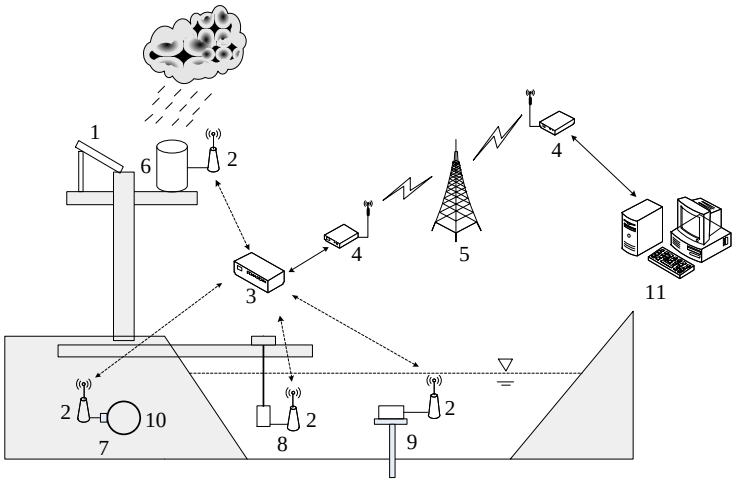

1: Solar power; 2: Sensor node; 3: Network coordinator; 4: GPRS module; 5: Base station; 6: FBG ombrometer; 7: FBG vibrometer; 8: FBG fluviograph; 9: FBG flowmeter; 10: Pipeline; 11: Monitoring terminal

Figure 6. Schematic diagram of the monitoring system

• GPRS network. It will be transmitted to the remote monitoring terminal that the monitoring data are aggregated in the network coordinator through GPRS network.

• Monitoring terminal. The GPRS module of upper computer is connected to the center server via RS-232 port, which is responsible for the real-time data storage, analysis and processing, and it will give an alarm signal when the critical values have been reached.

4.2 Hardware constitution of system

The hardware constitution of monitoring system is shown in Figure 7. The sensor nodes are composed of FBG ombrometer, FBG fluviograph, FBG flowmeter, FBG vibrometer, MCU module and radio frequency (RF) module, and they are responsible for real-time data acquisition and transmission in the monitoring area. After receiving the monitoring data, the each sensor node will convert them to digital signals and send them to the MCU module, and the MCU module is responsible for data processing and transmission. All the sensor nodes are powered by the solar batteries. The network coordinator includes RF module, MCU module and GPRS module, which is responsible for data gathering and processing of ZigBee network, data communication with lower computer and executing some instructions. The network coordinator is supplied by an external power source.

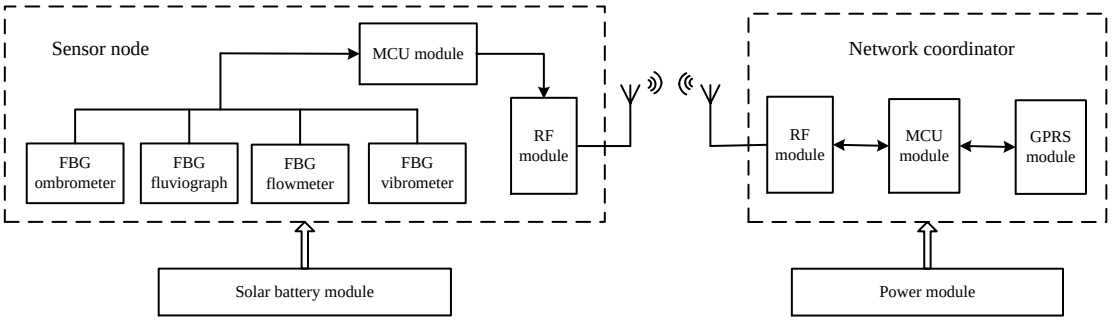

Figure 7. Hardware structure diagram of the monitoring system

The RF module adopts the CC2431, a radio frequency system with location detection hardware launched by Chipcon Company, which meets the technical regulations on ZigBee/IEEE 802.15.4 and is appropriate for a

variety of wireless network nodes related to ZigBee, including of tuner, router and terminal equipment. The CC2431 can realize the functions of data caching, read-write of status register with the work pattern of 4 SPI bus chip. The pins FIFO, FIFOP, CCA and SFD are used to set the transmitting or receiving register, controlling cleanup channel estimation and the clock or timing information input [17]. The pins CSn must always keep low level in the process of data transmission.

MCU module adopts the MSP430F1612 singlechip, a kind of ultra-low power mixed signal controller, which has normal work pattern (AM) and 4 low power pattern (LPMl, LPM2, LPM3, LPM4), and it is easy to accomplish the switch between the various work pattern. The MSP430F1612 is of high integration density and monolithic integration of multichannel 12 bit A/D conversion and on chip precision comparator. The interface circuit of CC2431 and MSP430F1612 singlechip is shown in Figure 8.

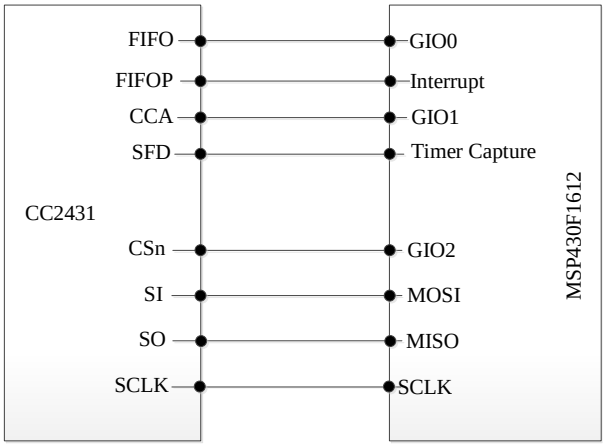

Figure 8. Interface circuit of RF module and MCU module

4.3 Fault tolerant features

The fault-tolerance features of this monitoring system adopts the top-down cluster tree structure-based VSN construction algorithm to construct a VSN with nodes of identical incidents monitored in sensor network deployment area[18]. In VSN, the incidents monitored are uploaded to the root node, and each cluster head node adds entry to the routing list during VSN cluster tree construction to form routing, so as to connect with all nodes with monitored identical incidents. When a sensor node in VSN is confirmed as fault node via fault-tolerant algorithm, the fault tolerance processing shown in Figure 9 will be performed. If S_i is the cluster head (CH) of VSN, any incident monitored by nodes within the cluster will be reported to CH and CH will be included within VSN incidents when CH loses the judgment. Thus, the loss of judgment of CH has little influence on whether the incident can be monitored. Nevertheless, to ensure that the wrong data submitted by CH in the case of loss of judgment does not affect the accuracy of the summarized data, such CH shall be deleted and a new CH shall be chosen immediately in the case of loss of judgment or wrong judgment.

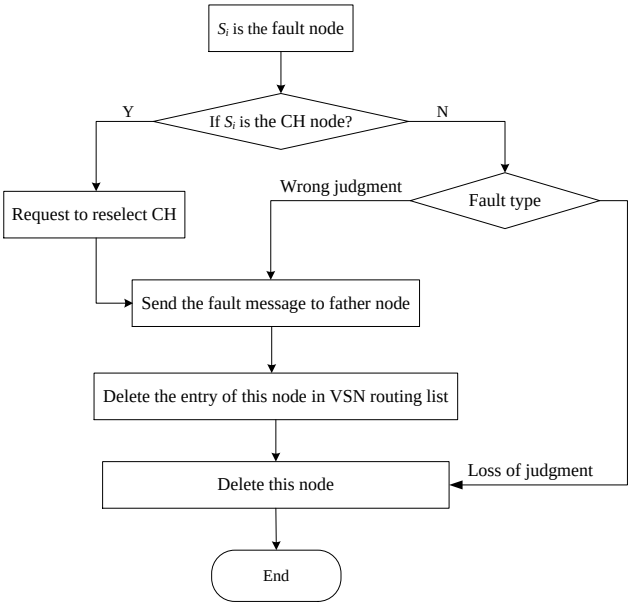

Figure 9. Fault node processing flow

5. PRACTICAL EXAMPLES

In order to validate the reliability of the monitoring system, field experiments were carried out on a gas pipeline in Langping River Valley of Changyang County, Hubei Province, in Central China, and the experimental results are shown in Figure 10~12. Figure 10 and Figure 11 show the monitoring curves of the water level and flow rate of the river in three-day sustained rainfall. It can be seen from the figures that the changes in water level and flow rate are obviously affected by the rainfall intensity. With the sustained rainfall and increase in rainfall intensity, the monitoring curves of the water level and flow rate appear 4 obvious peaks, while the changes in water level and flow rate are basically consistent with the change in rainfall intensity. The maximum water level appears in the 42th hour of continuous monitoring, up to 3.75m; the maximum flow rate appears in the 16th hour of continuous monitoring, up to 3.25m/s; the average water level and flow rate during rainfall period are 3.16m and 1.58m/s respectively. Figure 12 shows the vibration frequency monitoring curve of the pipeline. Monitoring point A is the measured value monitored by the sensor installed in lower suspended span pipeline section impacted by the flood, and monitoring point B is the measured value monitored by the sensor installed in the buried pipeline section. It can be seen from the figure that, protected by soil masses around, the buried pipeline sections are generally in static stable status, while impacted by the floor, the suspended pipeline sections have obvious vortex-induced vibration with the vibrational frequency change of -3.57~3.48Hz. Therefore, when the buried pipeline sections bare and suspend due to the washing by the flood, the vibration frequency will significantly increase, and measures shall be taken as soon as possible to avoid fatigue damage or pipeline break due to long-time vortex-induced vibration.

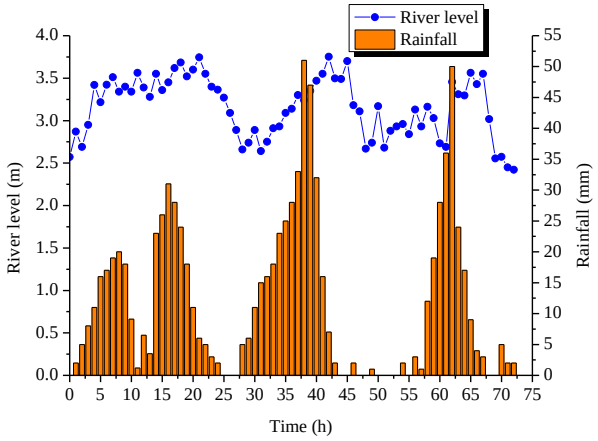

Figure 10. Curves of river level during three days of persistent rainfall

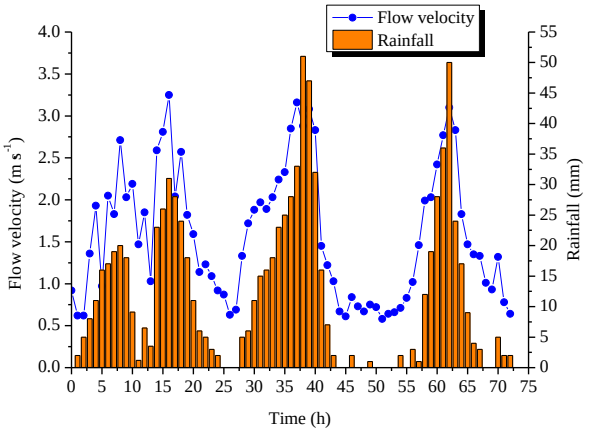

Figure 11. Curves of flow velocity during three days of persistent rainfall

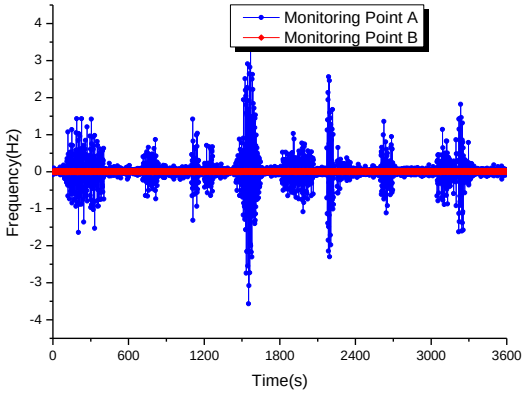

Figure 12. Frequency spectrum of pipeline subjected to flood scour

6. CONCLUSIONS

This article has designed a joint monitoring device of pipeline-flood by applying fiber Bragg grating sensing technology into hydrologic observation and vibration measurement field, which have the advantages of high accuracy, anti-electromagnetic interference, corrosion resistance, and the influence of temperature on measurement

results can be eliminated by using the dual-fiber pattern. In order to achieve the real-time and effective performances of data collection, the monitoring system is built on the basis of wireless network technology, that all the measurement points in field are linked to each other to make up monitoring network by using ZigBee technology, and the communication between center node of ZigBee and remote monitoring terminal has been realized by GPRS. Based on this monitoring system, we have carried out the field experiment on a gas pipeline laid in a river valley. The experiment results have proved that the system has the characteristics of flexible and fast networking, low power consumption, high reliability and unattended operation and can be applied well in practice.

ACKNOWLEDGEMENT

This research was supported by the National Quality Infrastructure (NQI) important special project under Grant JYZX201601000041.

REFERENCES

[1] Shuai Jian, Wang Xiaolin, Zuo Shangzhi. (2008).Breakage Action and Defend Measures to Pipeline under Geological Disaster. Welded Pipe and Tube, 31(5): 9-15(in Chinese)

[2] Zhao Yong. (2007). Optical fiber gratings and sensing technology. Beijing: Tsinghua University Press, 145(in Chinese)

[3] Rao Y J, Webb D J, Jackson D A. (1997). In fiber Bragg grating temperature sensor system for medical application. Journal of Lightwave Technology, 15(5): 779–785

[4] Mandal J, Pal S, Sun T. (2004). Bragg grating-based fiber-optic laser probe for temperature sensing. IEEE Photonics Technology Letters, 16(1): 218-220

[5] Chan Peter K C, Jin W, Lau K T. (2000). Multi-point strain measurement of composite-bonded concrete materials with a RF-band FMCW multiplexed FBG sensor array. Sensors and Actuators, 87: 19-25

[6] GUAN Shouhua, YU Qingxu, SONG Shide. (2005). Experimental Study on Concentration Sensor Based on Long-Period Fiber Grating with Single Head. Journal of Transduction Technology, 18(3): 653-656(in Chinese)

[7] Yao Yuan, Yi Benshun, Dong Xiaopeng, Zou Yi, Xiao Jinsheng. (2008). Fiber Bragg Grating AC Current Measurement Based on Twin-Core Fiber Filter. Journal of Transduction Technology, 21(6): 1070-1074(in Chinese)

[8] Davino D, Visone C, Ambrosino C. (2008). Compensation of Hysteresis in Magnetic Field Sensors Employing Fiber Bragg Grating and Magneto-Elastic Materials. Sensors and Actuators A, 147: 127-136

[9] Poopalan P, Thant M, Harun S. (2009). High sensitivity fiber Bragg grating pressure sensor using thin metal diaphragm. IEEE Sensors Journal, 9(12): 1654-1659

[10] Mita A, Yokoi L. (2000). Fiber Bragg grating accelerometer for structural health monitoring. Fifth International Conference on Motion and Vibration Control (MOVIC 2000), 4-8

[11] Sun An, Qiao Xueguang, Jia Zhenan, Guo Tuan, Chen Changyong. (2004). Strain Response of a Special Cantilever-based Fibre Bragg Grating. Journal of Optoelectronics•laser, 15(2): 153-155(in Chinese)

[12] Tarun K G. (2004). Prospects for Fibre Bragg Gratings and fabry-perot interferometers in fibre-optic vibration sensing. Sensors and Actuators A, 113(1): 20-38

[13] Mitsui T, Hosoe K, Usami H. (1987). Development of fiber optic voltage sensors and magnetic field sensors. IEEE Trans. Power Delivery, , 2(1):87-93

[14] Kersey A D, Davis M A, Patrick H J. (1997). Fiber grating sensors. Light wave Technol, 15(8): 1442-1463

[15] Yi B, Chu B C, Chiang K S. (2003). Temperature compensation for a Fiber-Bragg-Grating-based magnetostrictive sensor. Microwave and Optical Technology letters, 36(3): 211-213

[16] Tang Huiqiang, Zhu Jiacong. (2009). Pressure Pluviometer Based on Wireless Sensor Network. Communications Technology, 42(3): 247-249(in Chinese)

[17] Li Haosheng, Wang Ruchuan, Sha Chao. (2008). Design of Wireless Sensor Newwork Node Based on CC2431. Electronic Engneer, 34(12): 63-66(in Chinese)

[18] H M N Bandara，A P Jayasumana，T H Illangasekare. (2008). Cluster tree based self organiza tion of virtual sensor networks.IEEE Globecom Workshops: 1-6